Geochemistry, Geophysics, Geosystems

Supporting Information for

Formation and structures of horizontal submarine fluid conduit and venting systems associated with marine seeps

Luis A. M. Rocha[1], Carlos Gutiérrez-Ariza[2], Carlos Pimentel[2], Isabel Sánchez-Almazo[3], C. Ignacio Sainz-Díaz[2], Silvana S. S. Cardoso[1], Julyan H. E. Cartwright[2,4]

[1]Department of Chemical Engineering and Biotechnology, University of Cambridge, Cambridge CB2 3RA, UK
[2]Instituto Andaluz de Ciencias de la Terra, CSIC-Universidad de Granada, 18100 Armilla, Granada, Spain
[3]Centro de Instrumentación Científica, Universidad de Granada, Av. Fuentenueva, 18071 Granada, Spain
[4]Instituto Carlos I de Física Teórica y Computacional, Universidad de Granada, 18071 Granada, Spain

Contents of this file

Additional Supporting Information (Files uploaded separately)

Introduction

The supporting information includes additional information about the analytical techniques used in this work, as well as additional figures and a movie, complementary to the information and figures in the main article.

Text S1. Analytical Techniques

The Scanning Electron Microscopy (SEM) studies of the polished thin sections of both chimneys were performed using a Thermofisher-FEI Quanta 650 FEG located at the Centro de Instrumentación Científica of the University of Granada. Elemental maps were acquired by two Bruker XFlash® 6 | 30 SSD EDS equipped with Esprit 1.9 software at 20 KV of acceleration voltage and about 10mm of working distance. A CBS (Circular Backscatter Detector) was used for compositional BSE image acquisition. Micro-Raman spectroscopy analyses were performed with a JASCO NRS-5100 spectrometer connected to a microscope with a objective lens 100x, using a visible/near-infrared (VIS-NIR) laser of 785 nm and 28.8 mW using 10 acquisition cycles of 30 s (Fig. S1a, S1b). In some cases the power of the laser was too strong and destroyed the sample, then an additional attenuation was applied getting a power of 4.7 mW (Fig. S1c). Powder X-ray diffraction analysis were performed using a Bruker D8 Discover microfocus diffractometer with detector PILATUS3R 100KA with the Cu K-α wavelength was also used. The identification of the crystallographic phases in the diffractograms was performed with the X-Powder program (J.D. Martin, http://www.XPowder.com/index.html, 2004).
X-ray computed tomography (XCT) was performed in an Xradia 510 VERSA4. Taking into account the size and density of the sample a 0.4X (Wide-Field-Mode) detector was used with a voltage, target power and exposure time set to 140 kV, 10 W and 17 s respectively and achieved pixel size of 26.3 µm. Data processing was performed using Scout and Scan Control System 12.0.8059 and Reconstructor Scout and Scan 12.0.8059. Further data treatment and visualization were carried out with FIJI distribution of ImageJ including 3DViewer plugin.

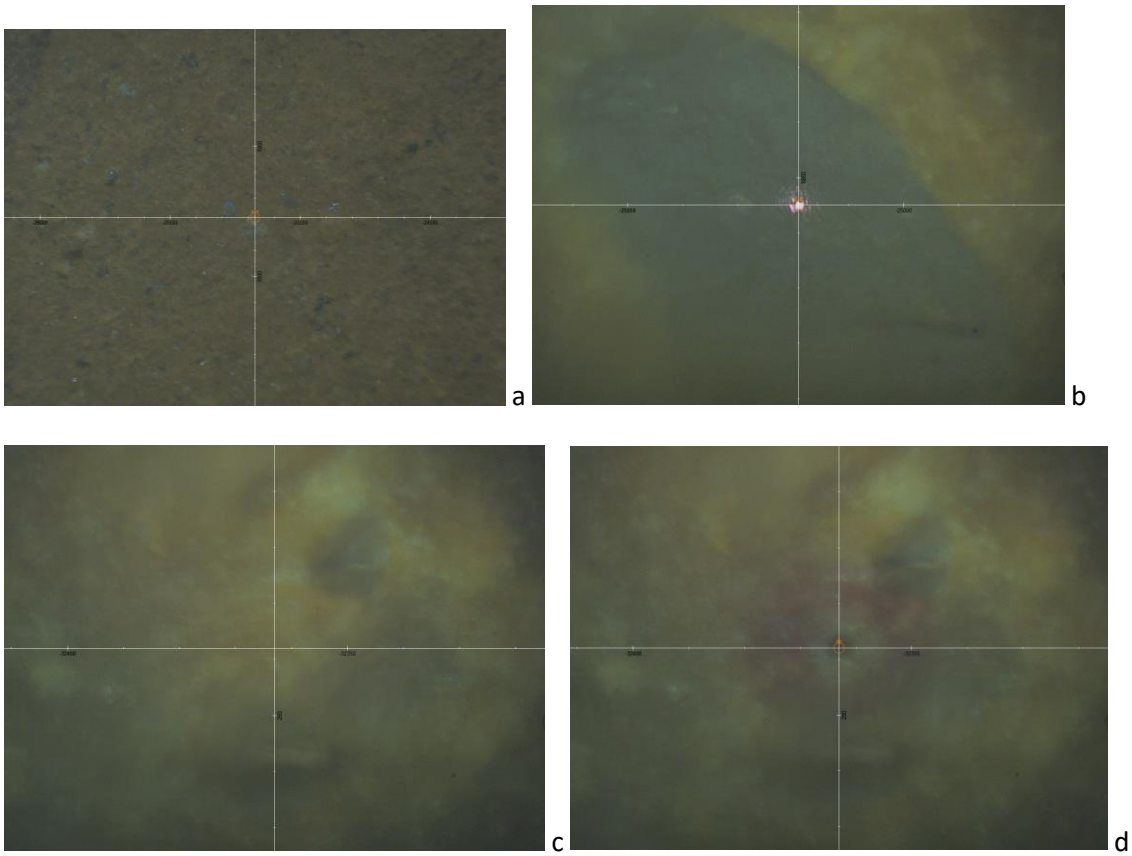

Figure S1. Sample for microRaman analysis of a section of a spiral chimney of Cadiz Gulf. (a) General Zone; (b) a gray particle; (c) an ocher zone; (d) the same former zone after the laser damage.

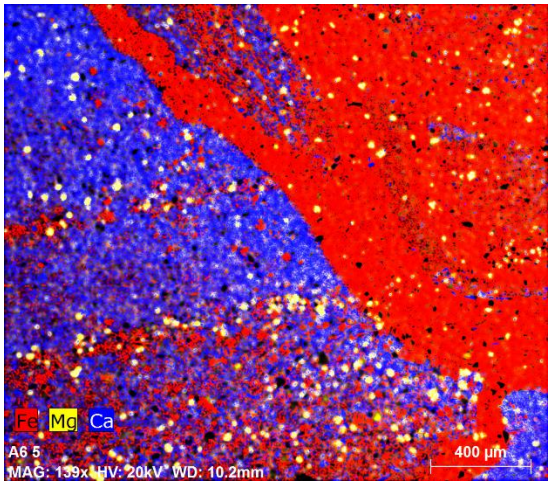
Fe Mg Ca
A6 5
MAG: 139x HV: 20kV WD: 10.2mm
400 µm
a

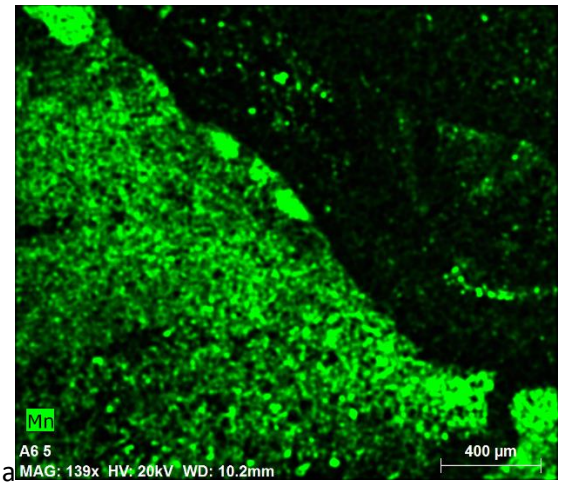
Mn
A6 5
MAG: 139x HV: 20kV WD: 10.2mm
400 µm
b

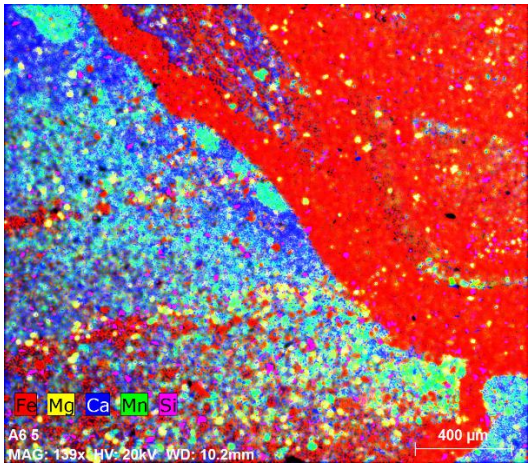
Fe Mg Ca Mn Si
A6 5
MAG: 139x HV: 20kV WD: 10.2mm
400 µm
c

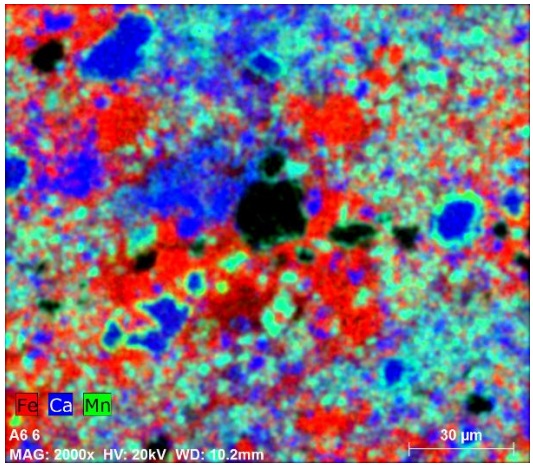
Fe Ca Mn
A6 6
MAG: 2000x HV: 20kV WD: 10.2mm
30 µm
d

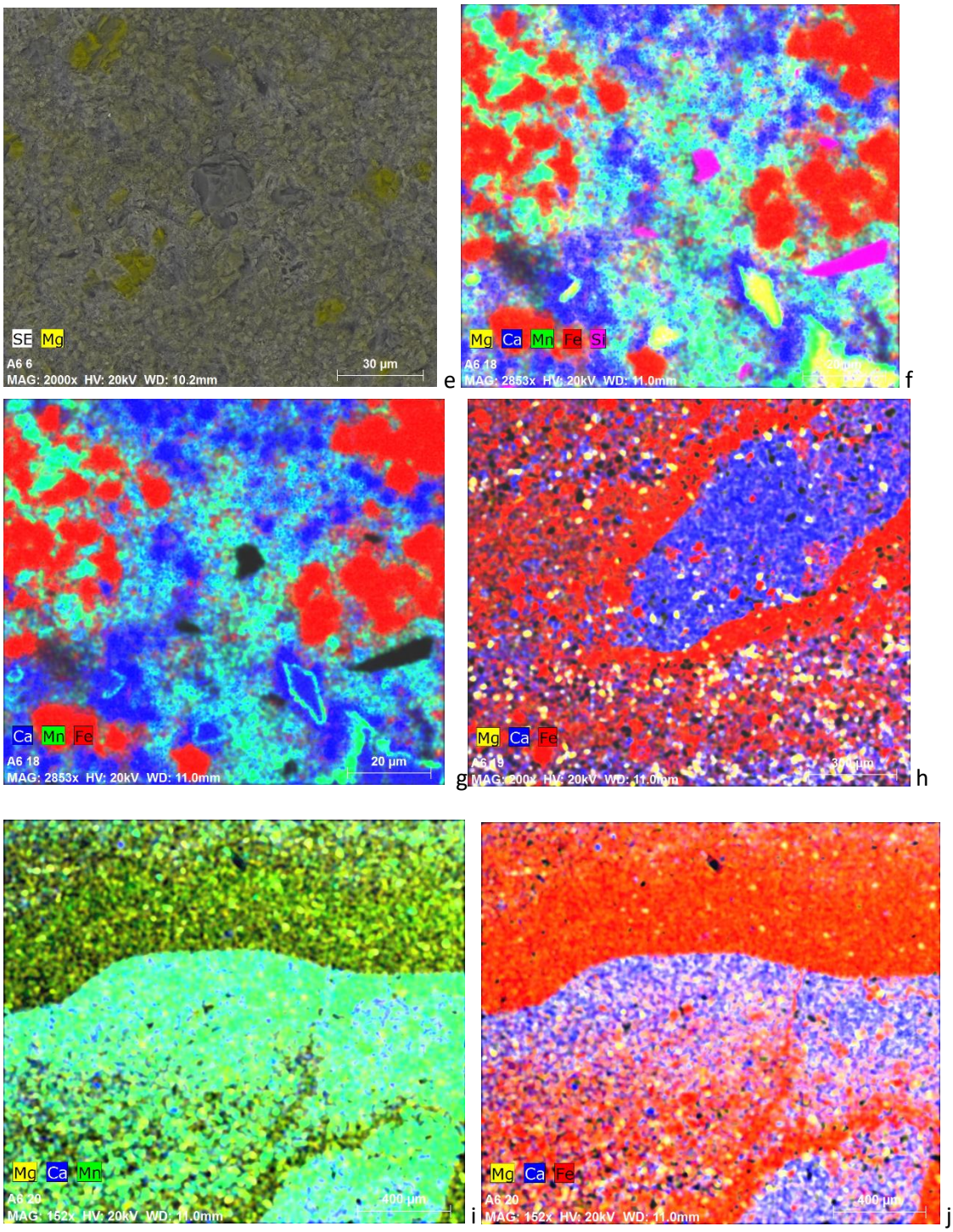

Figure S2. Analytical EDX maps of partial element compositions of regions from a polished thin layer of a section of the cylindrical chimney. Complementary to the Fig. 8. (a,b,c) Partial compositional mapping of Fig. 8a; (d,e) Partial compositional mapping of

Fig. 8d; (f,g) Partial compositional mapping of Fig. 8e; (h) Partial compositional mapping of Fig. 8f; (i,j) Partial compositional mapping of Fig. 8h.

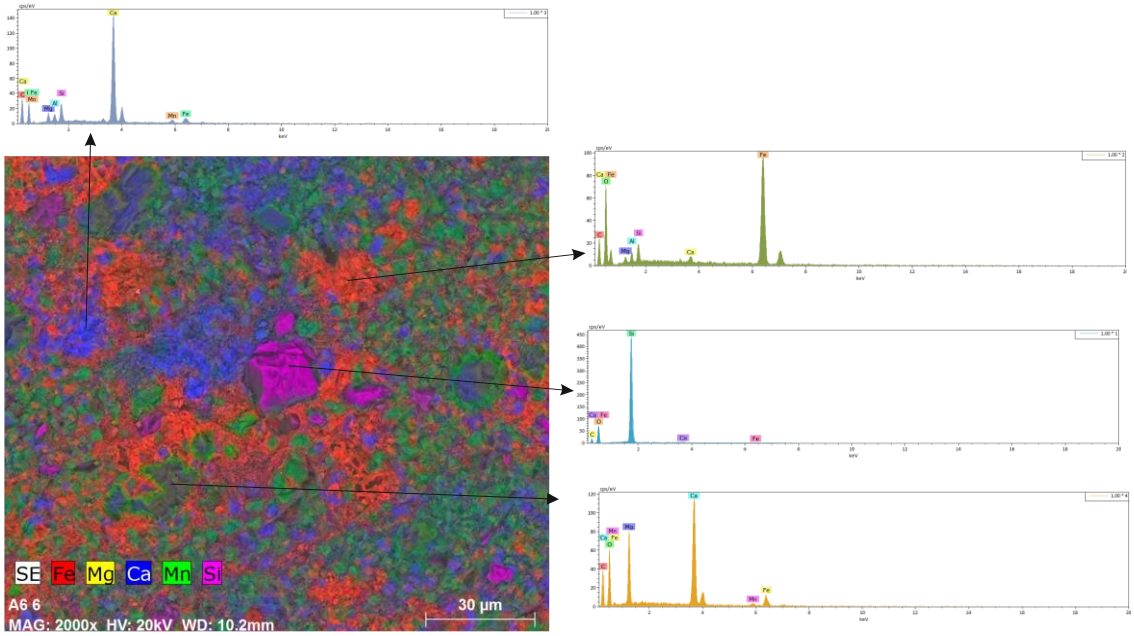

Figure S3. Chemical analysis of the one region riched in Ca of a thin polished layer from a section of the cylindrical chimney showed in Fig. 8d.

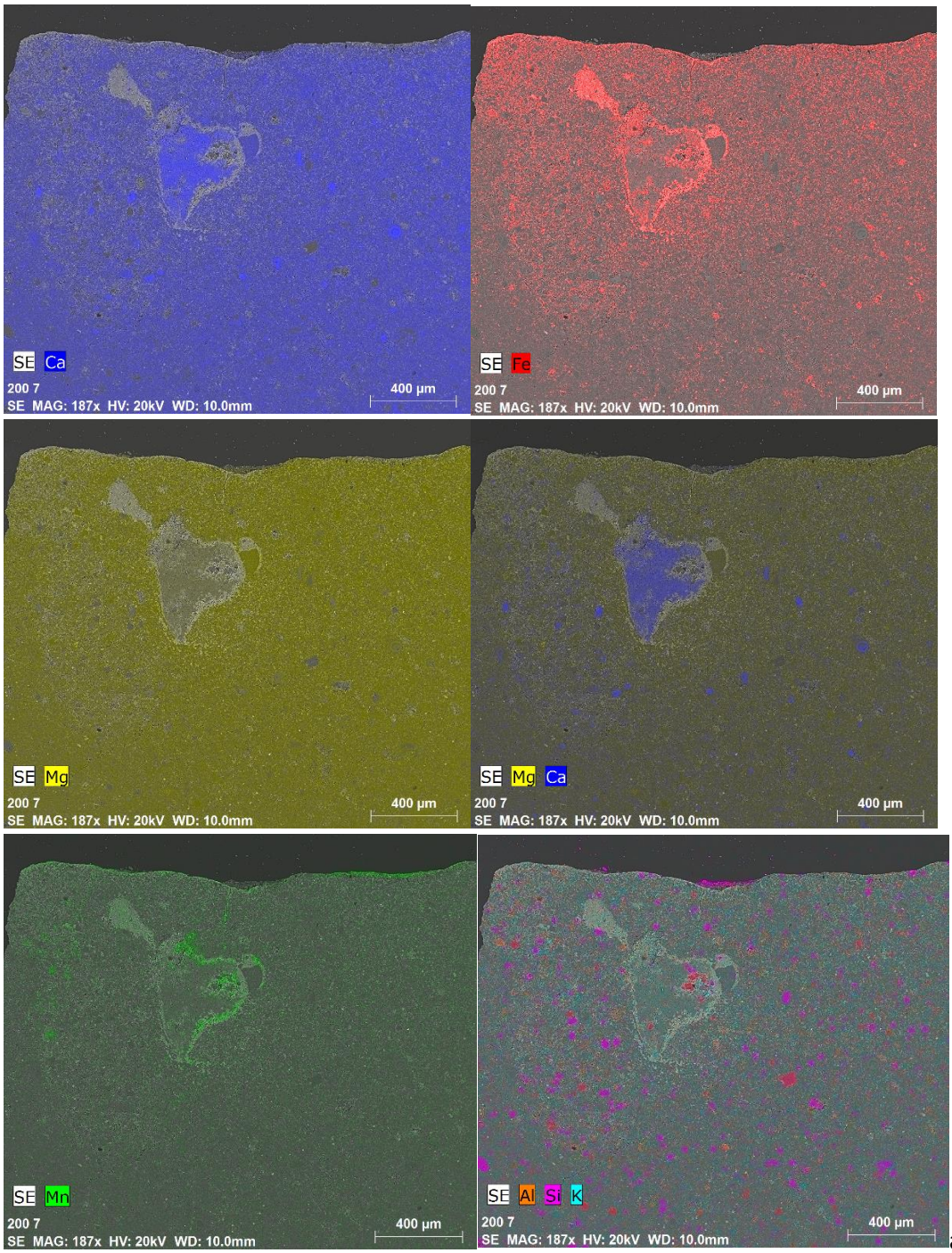
SE Ca
200 7
SE MAG: 187x HV: 20kV WD: 10.0mm
400 µm
SE Fe
200 7
SE MAG: 187x HV: 20kV WD: 10.0mm
400 µm
SE Mg
200 7
SE MAG: 187x HV: 20kV WD: 10.0mm
400 µm
SE Mg Ca
200 7
SE MAG: 187x HV: 20kV WD: 10.0mm
400 µm
SE Mn
200 7
SE MAG: 187x HV: 20kV WD: 10.0mm
400 µm
SE Al Si K
200 7
SE MAG: 187x HV: 20kV WD: 10.0mm
400 µm
a

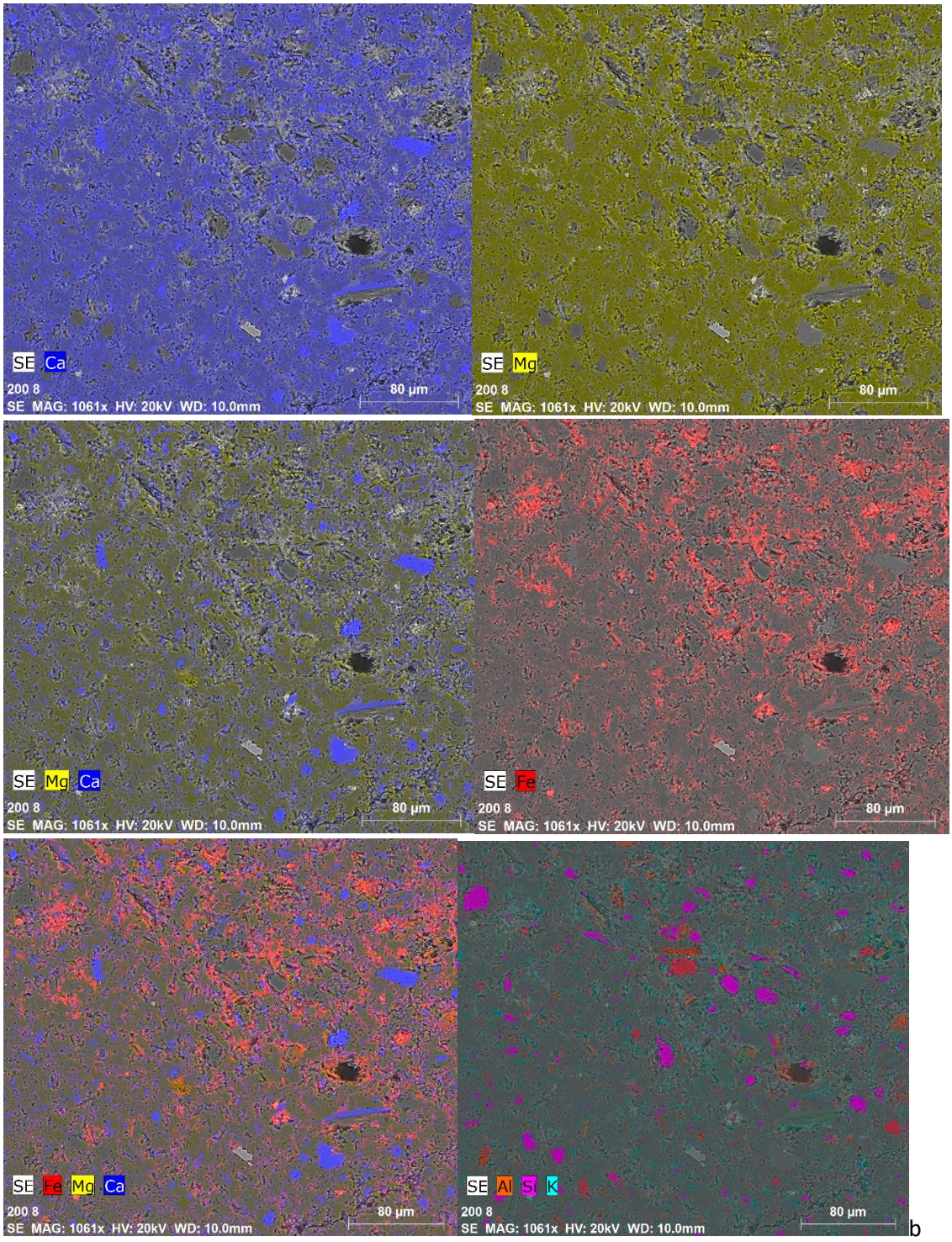
SE Ca
200 8
SE MAG: 1061x HV: 20kV WD: 10.0mm
80 µm
SE Mg
200 8
SE MAG: 1061x HV: 20kV WD: 10.0mm
80 µm
SE Mg Ca
200 8
SE MAG: 1061x HV: 20kV WD: 10.0mm
80 µm
SE Fe
200 8
SE MAG: 1061x HV: 20kV WD: 10.0mm
80 µm
SE Fe Mg Ca
200 8
SE MAG: 1061x HV: 20kV WD: 10.0mm
80 µm
SE Al Si K
200 8
SE MAG: 1061x HV: 20kV WD: 10.0mm
80 µm
b

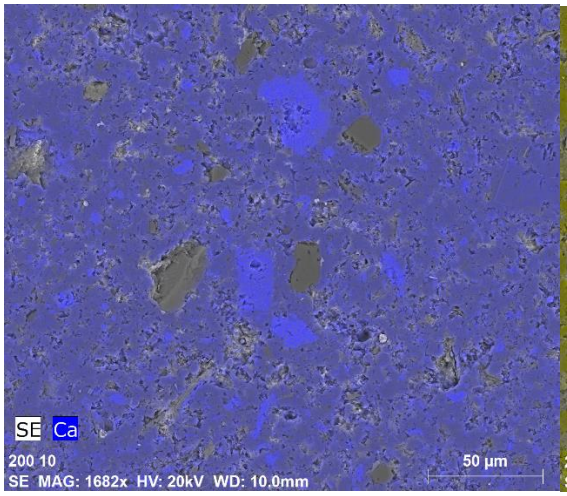
SE Ca
200 10
SE MAG: 1682x HV: 20kV WD: 10.0mm
50 µm

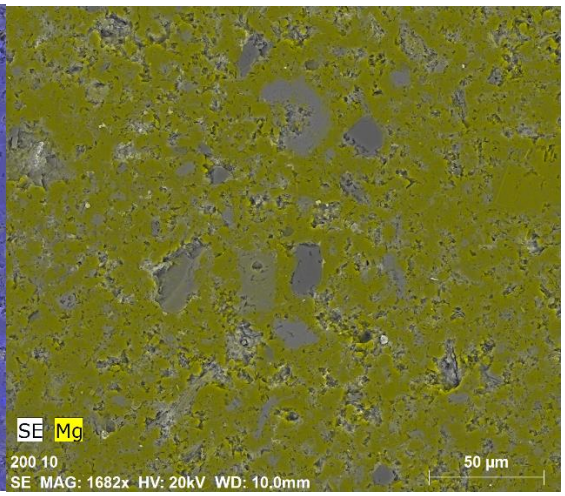
SE Mg
200 10
SE MAG: 1682x HV: 20kV WD: 10.0mm
50 µm

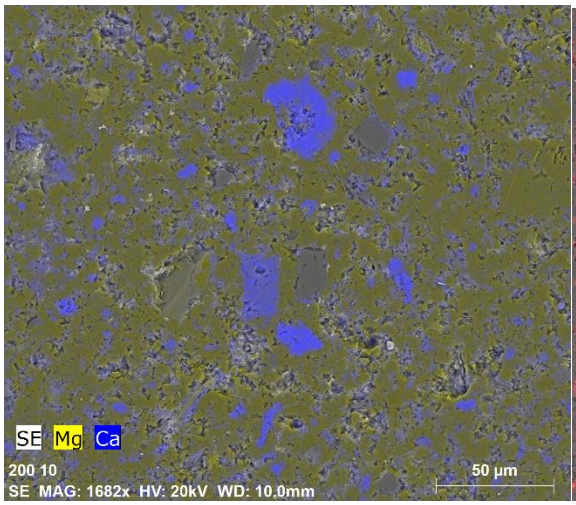
SE Mg Ca
200 10
SE MAG: 1682x HV: 20kV WD: 10.0mm
50 µm

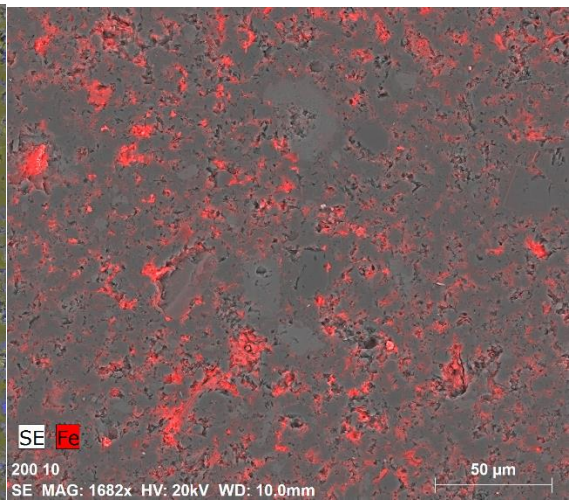
SE Fe
200 10
SE MAG: 1682x HV: 20kV WD: 10.0mm
50 µm

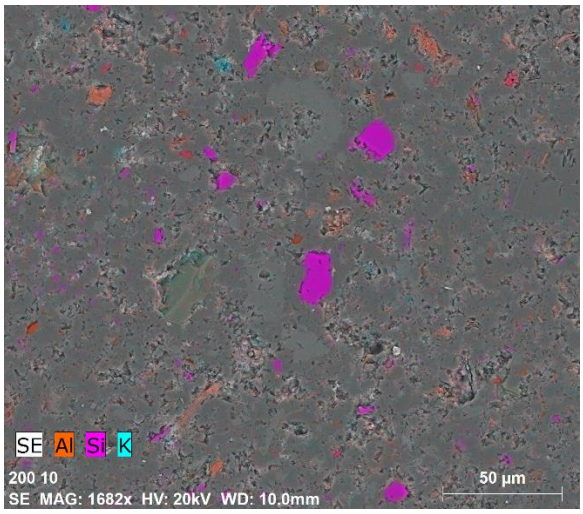
SE Al Si K
200 10
SE MAG: 1682x HV: 20kV WD: 10.0mm
50 µm

c

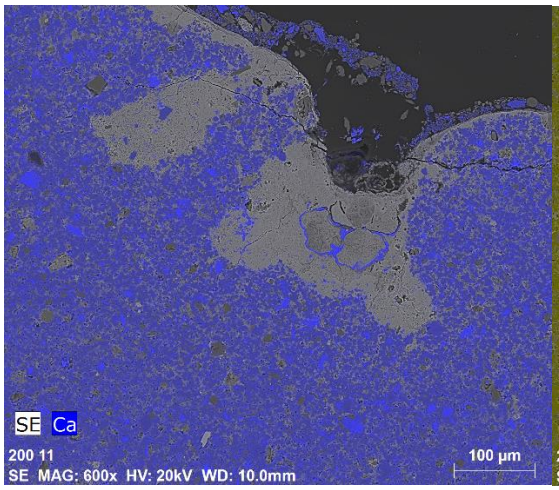
SE Ca
200 11
SE MAG: 600x HV: 20kV WD: 10.0mm
100 µm

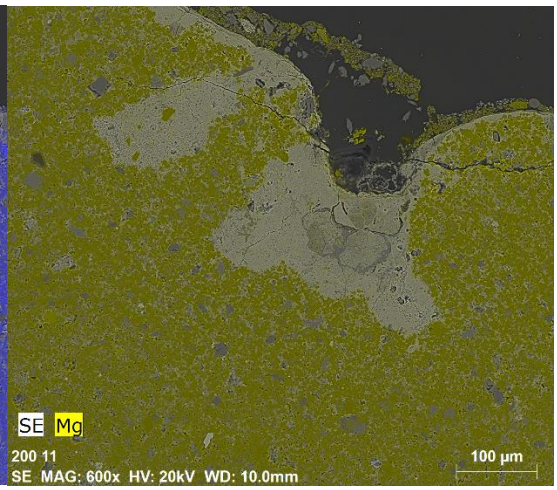
SE Mg
200 11
SE MAG: 600x HV: 20kV WD: 10.0mm
100 µm

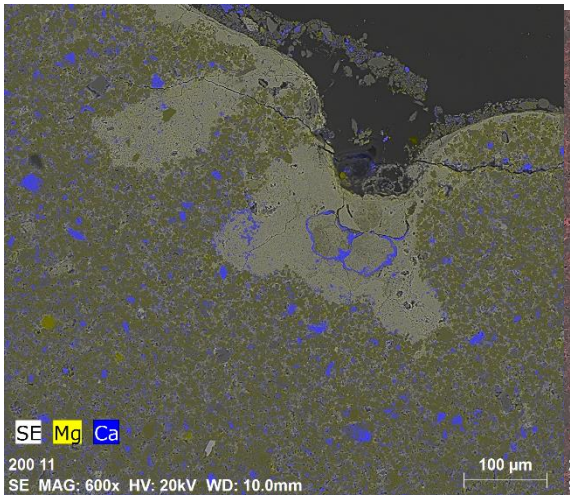
SE Mg Ca
200 11
SE MAG: 600x HV: 20kV WD: 10.0mm
100 µm

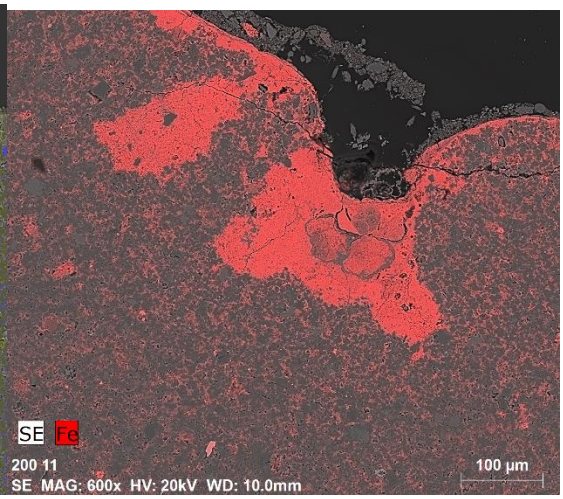
SE Fe
200 11
SE MAG: 600x HV: 20kV WD: 10.0mm
100 µm

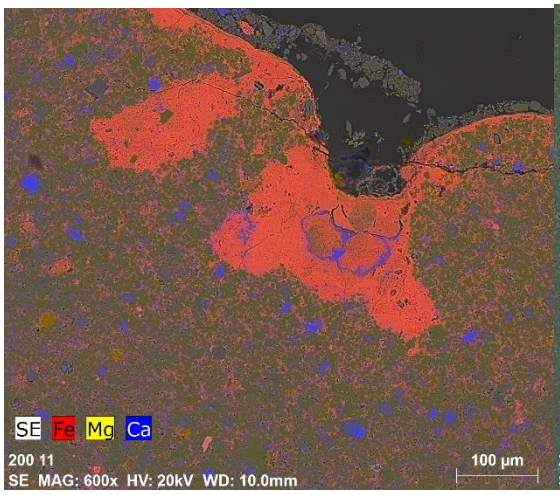
SE Fe Mg Ca
200 11
SE MAG: 600x HV: 20kV WD: 10.0mm
100 µm

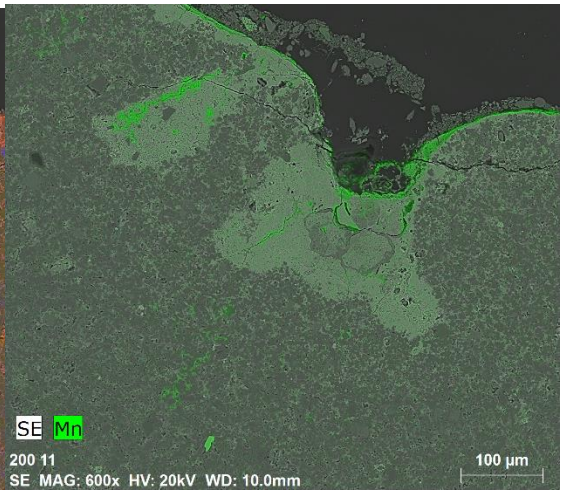
SE Mn
200 11
SE MAG: 600x HV: 20kV WD: 10.0mm
100 µm

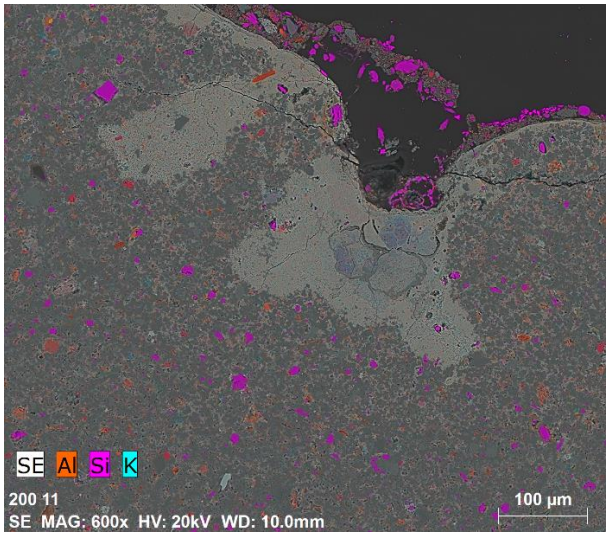
SE Al Si K
200 11
SE MAG: 600x HV: 20kV WD: 10.0mm
100 µm
d

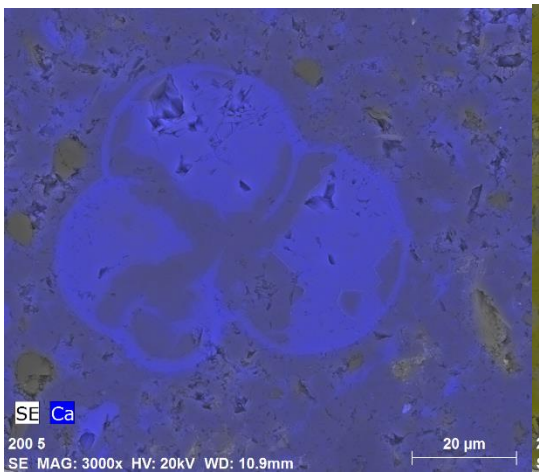
SE Ca
200 5
SE MAG: 3000x HV: 20kV WD: 10.9mm
20 µm

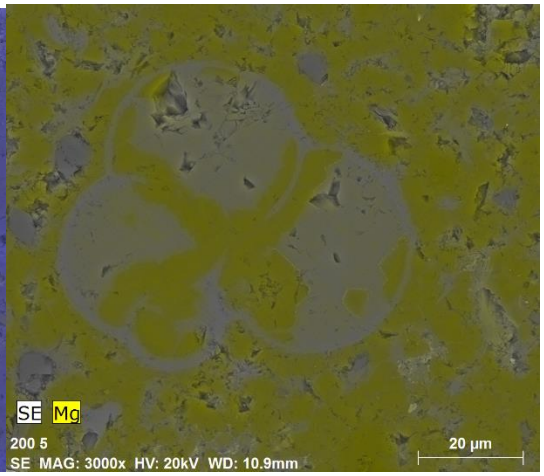
SE Mg
200 5
SE MAG: 3000x HV: 20kV WD: 10.9mm
20 µm

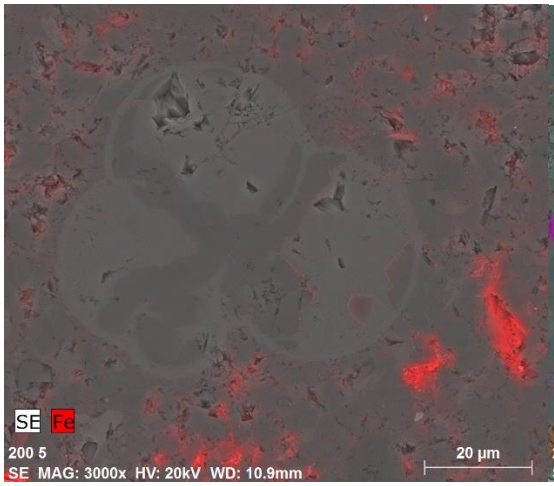
SE Fe
200 5
SE MAG: 3000x HV: 20kV WD: 10.9mm
20 µm

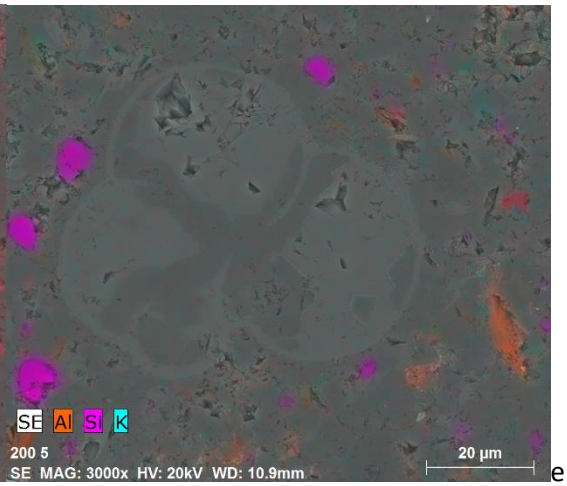
SE Al Si K
200 5
SE MAG: 3000x HV: 20kV WD: 10.9mm
20 µm
e

Figure S4. Analytical EDX maps of partial element compositions of five zones of a section of the spiral chimney from Fig. 9.

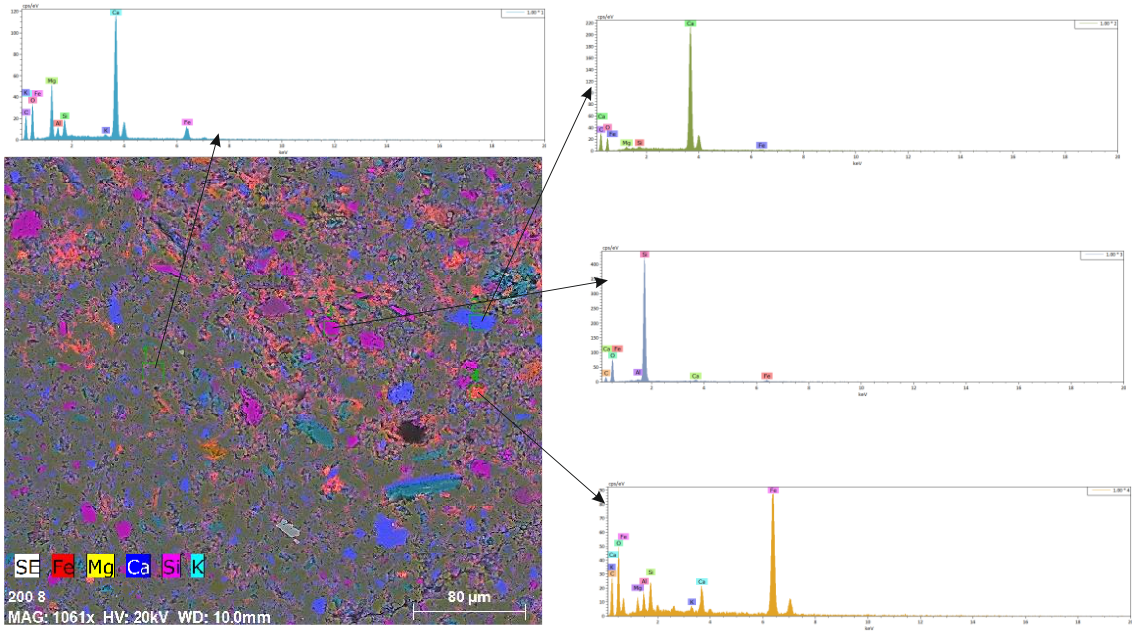

Figure S5. Chemical analysis of a section of the spiral chimney showed in Fig. 9b.

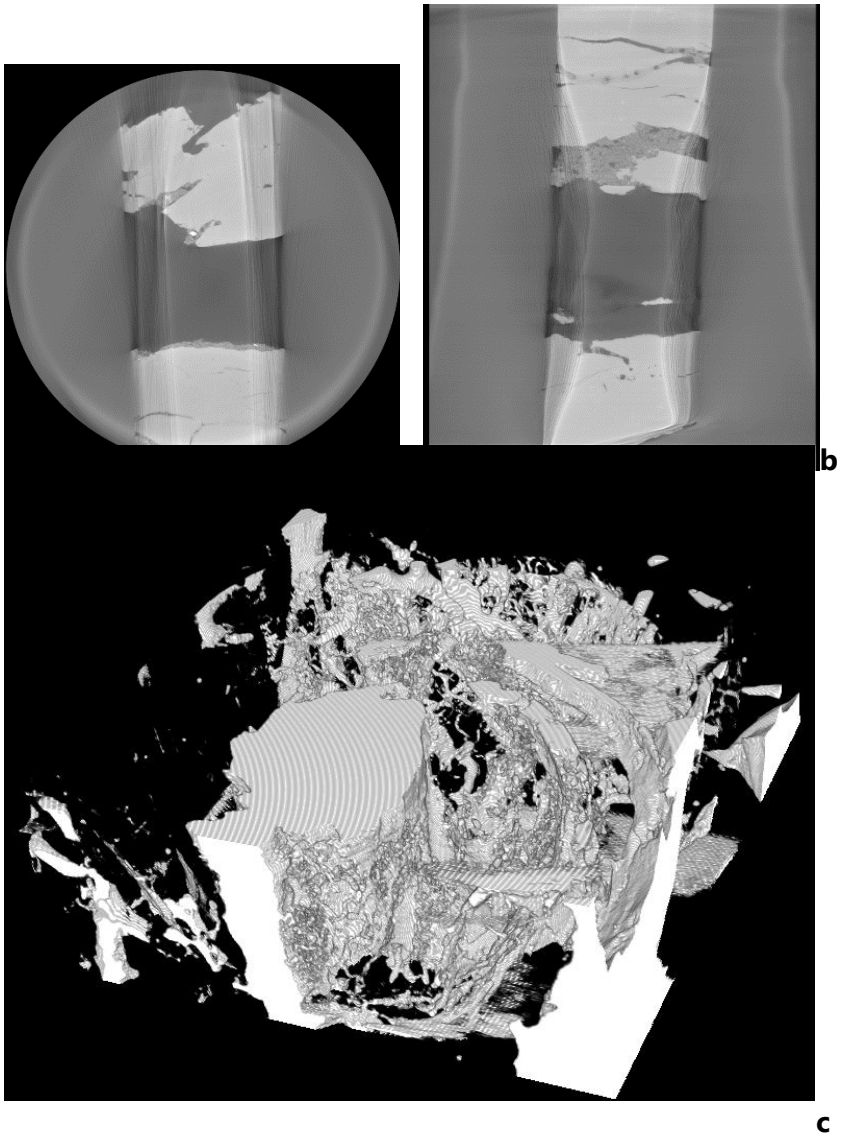

Figure S6. 3D-x-ray tomography of a lateral view of the helicoidal chimney (a,b) and a negative composition observing the hollow zone and the helicoidal configuration (c).

Movie S1. X-ray tomography images complementary to image S6.